Composites: Part A 40 (2009) 954–967

Contents lists available at ScienceDirect

Composites: Part A

journal homepage: www.elsevier.com/locate/compositesa

Damage resistance and tolerance of carbon/epoxy composite coupons subjected to simulated lightning strike

Paolo Feraboli *, Mark Miller

Department of Aeronautics and Astronautics, Box 352400, Guggenheim Hall, University of Washington, Seattle, WA 98195-2400, United States

ARTICLE INFO

Article history:
Received 11 November 2008
Received in revised form 9 April 2009
Accepted 21 April 2009

Keywords:
Damage resistance
B. Damage tolerance
Lightning strike
A. Carbon fiber

ABSTRACT

Damage is inflicted in a series of carbon fiber/epoxy composite specimens using a simulated lightning strike generator in the effort to understand the fundamental damage response of this material form. The strikes up to 50,000 A and 28,000 V are inflicted on both pristine specimens and specimens containing a Hilok stainless steel fastener. Damage area is evaluated via ultrasonic scanning, and advanced optical microscopy is used to gain further understanding in the morphology of damage. Subsequent mechanical testing to assess the residual tensile and compressive strength and modulus of the material is performed according to ASTM standards. Results show that residual tension strength counter intuitively increases after the infliction of damage, while residual compressive strength is much more dramatically and negatively affected. Furthermore, the presence of the fastener influences dramatically both the state of damage in the specimen and its residual strength by spreading throughout the thickness rather than limiting it to the specimen surface.

1. Introduction

A wide range of composite material forms are finding use in today's aerospace, automotive, and other transportation industry segments. These materials are finally fulfilling the promise of providing original equipment manufacturers (OEM's) with a cost-competitive alternative to metallic materials. The Boeing 787 dreamliner, due to join the world's active fleet by mid 2009, features over 50% carbon fiber reinforced polymers (CFRP) by structural weight [1]. Beside the direct benefits resulting from the greater specific mechanical properties, such as increased fuel efficiency, and reduced pollutant and acoustic emissions, other indirect advantages of a CFRP-intensive airframe are reduced maintenance requirements, and increased passenger comfort due to the superior fatigue- and corrosion-resistance characteristics of these materials. However, the introduction of composites in the primary structure of modern aircraft presents special problems with regards to the lighting strike threat. While metallic structures, such as traditional aluminum airframes, are highly conductive, CFRP have a much lower electrical conductivity. Although carbon fibers are good conductors, the polymer matrix is an excellent dielectric and therefore reduces the overall conductivity of the composite laminate.

Lightning strike is a threat to all structures, whether metallic or composites, and requires careful consideration from a certification standpoint. Lightning can induce damage on a aircraft structure, both metallic and composite, by melting or burning at lightning attachment points, resistive heating, magnetic force effects, acoustic shock, arcing and sparking at joints, and ignition of vapors in fuel tanks [2,3]. The main focus of direct lightning strike threat studies to date has been on its potential to arc and generate a spark (ignition studies). However, little research in the public domain has been done in order to assess the potential losses in structural integrity of the CFRP structure due to the lightning strike damage. Published research has focused on the comparative behavior of protected and unprotected panels of glass and carbon fiber composites, mostly in sandwich form, under simulated lightning strike. The work has focused on visual and non-destructive inspection aimed at assessing inspection and repair procedures for representative aircraft structures [2–5]. Limited work was published in [6] to assess the structural performance of CFRP specimens following lightning strike damage, and it attempted to provide a comparison with the damage due to other sources of mechanical damage, such as machined notches. Recent work is being conducted to assess the use of novel protection systems, such as the introduction of conductive carbon nanotubes, to reduce the lightning strike damage and to replace current protection systems, such as copper strips and interwoven conductive wires [7].

Of particular interest to CFRP or other conductive composites is damage resulting from acoustic shock and resistive heating. When lightning strikes, a large amount of energy is delivered very rapidly, causing the ionized channel to expand with supersonic speed. If the shockwave encounters a hard surface its kinetic energy is transformed into a pressure rise, which causes fragmentation of the structure. On the other hand, resistive heating leads to

* Corresponding author. Tel.: +1 206 543 2170; fax: +1 206 543 0217.
E-mail address: feraboli@u.washington.edu (P. Feraboli).

1359-835X/$ - see front matter © 2009 Elsevier Ltd. All rights reserved.
doi:10.1016/j.compositesa.2009.04.025

temperatures rise, and in turn it initiates a breakdown of the resin/fiber interface by pyrolysis. If the gases developing from the burning resins are trapped in a substrate, explosive release may occur with subsequent damage to the structure.

The primary objectives of designing against lightning direct effects are to prevent catastrophic structural damage, prevent hazardous electrical shocks to occupants, prevent loss of aircraft flight control capability, and to prevent ignition of fuel vapors. The basic lightning protection regulation for airframes is the same for all vehicle categories, and appears in the Federal Aviation Administration Advisory Circular AC 25–21, Section 25.581 "Lightning Protection of Structure" [8], which requires that the aircraft be able to sustain a lightning strike without experiencing catastrophic damage. For nonmetallic components, compliance may be shown by designing the components to minimize the effect of a strike or incorporating acceptable means of diverting the resulting electrical current so as not to endanger the airplane. These requirements are inherently non-specific, and allow manufacturers to adopt different certification strategies. However, SAE provides aerospace recommended practices (ARP) that can be utilized to show compliance with these requirements.

According to SAE ARP 5414 [9], the surface of an aircraft can be divided into a set of three regions called lightning strike zones, which represent the areas likely to experience the various types of lightning currents. Lightning zoning is a functional step in demonstrating that the aircraft is adequately protected from both direct and indirect effects of lightning. Zone 1 regions are likely to experience initial lightning attachment and first return strokes, while Zone 2 regions are likely to experience subsequent swept strokes, or re-strikes. Except for a few protruding areas of the airframe, such as the wing tips and nose, which comprise Zone 1, the vast majority of the airframe belongs to Zone 2, as shown in color green in Fig. 1.

According to SAE ARP 5412 [10], four current components (A–D) comprise the lightning flash current waveforms recommended for evaluating direct effects, Fig. 2. Component A represents the first return stroke, current components B and C represent the lightning environment that might be caused by the intermediate and long duration currents following some return strokes or re-strikes, and current component D represents a subsequent stroke. It can be seen from Fig. 2, which is not to scale, that components B and C exhibit much lower peak amplitudes than components A and D, but a very high charge transfer. B and C can be thought as currents that act as a bridge between the initial stroke A and the subsequent one D. Current waveform A is reserved for Zone 1 regions, while Zone 2 regions are required to sustain only current waveform D, while both are required to sustain B and C current components.

These waveforms represent idealized environments, which are to be applied to the aircraft for purposes of analysis and testing. The waveforms are not intended to replicate a specific lightning event, but they are intended to be composite waveforms whose

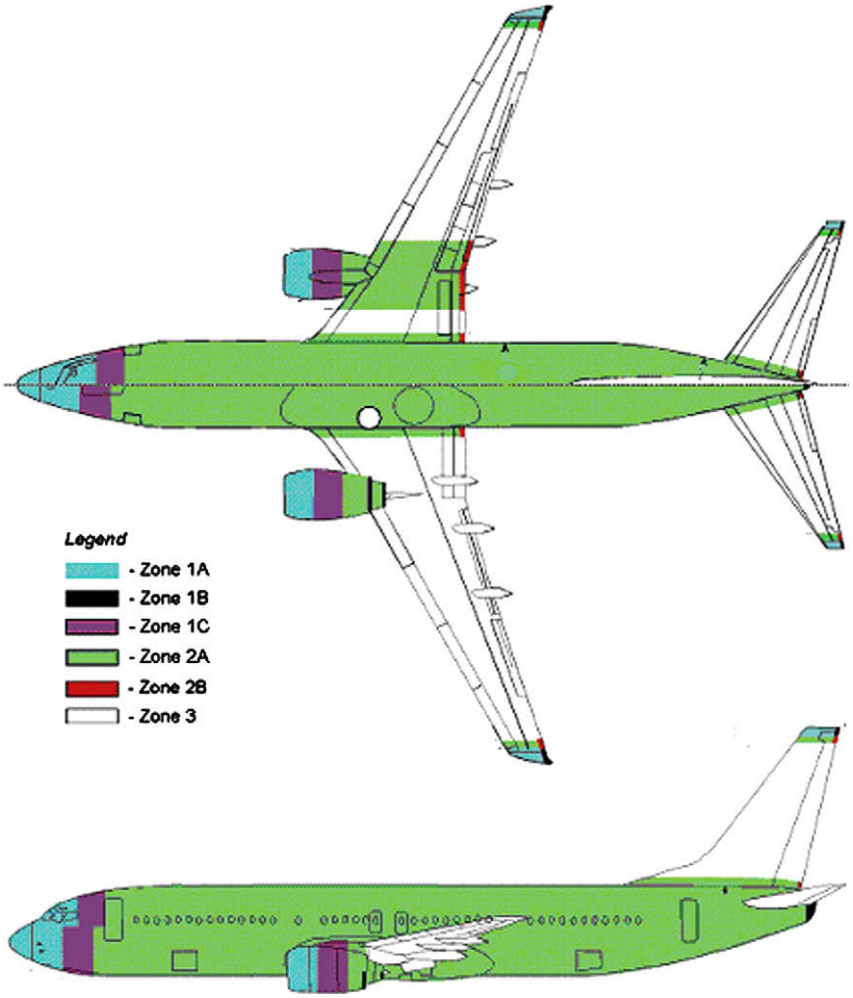

Fig. 1. Lightning zoning diagram for a typical large commercial transport per SAE 5414.

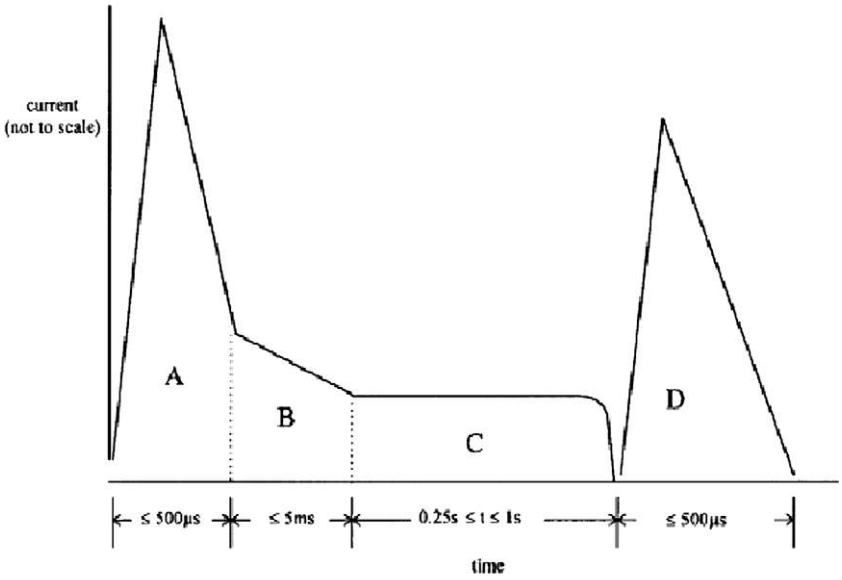

COMPONENT A (First Return Stroke)

Peak Amplitude	:	200kA (± 10%)
Action Integral	:	2 x 10^6A^{2}s (± 20%) (in 500µs)
Time Duration	:	≤ 500µs

COMPONENT B (Intermediate Current)

Max. Charge Transfer	:	10 Coulombs (± 10%)
Average Amplitude	:	2kA (± 20%)
Time Duration	:	≤ 5ms

COMPONENT C (Continuing Current)

Amplitude	:	200 - 800A
Charge Transfer	:	200 Coulombs (± 20%)
Time Duration	:	0.25 to 1 s

COMPONENT D (Subsequent Return Stroke)

Peak Amplitude	:	100kA (± 10%)
Action Integral	:	0.25 x 10^6A^{2}s (± 20%) (in 500µs)
Time Duration	:	≤ 500µs

Fig. 2. Typical simulated lightning current waveforms per SAE 5412.

effects upon aircraft are those expected from natural lightning. For each waveform, peak current amplitude, action integral and time duration are the primary parameters that dictate the response of the structure. The action integral is a measure of the intensity of the strike, and therefore to ensure that the strike accurately simulates the real lightning event, it is important to ensure that such quantity is as high as specified by the requirements.

While regulatory agencies impose compliance with zoning procedures, aircraft manufacturers also have internal requirements that address both safety and economic concerns. In a fashion similar to foreign object damage (FOD), whereby detection thresholds such as BVID (barely visible impact damage) or VID (visible impact damage) are set to determine maintenance and inspection procedures, different repair scenarios exist for lightning strike damage. Table 1 summarizes the types of lightning strike that are of interest to airframe manufacturers, which range from 10 to 50 kA, hence below the 100 kA and 200 kA requirements of current waveforms D and A, respectively.

This paper is focused around assessing the damage resistance and tolerance capabilities of structural carbon/epoxy prepreg tape specimens subjected to simulated lightning strike in the range of 10–50 kA, which are adequate currents to inflict damage on coupon-level specimens. The study is aimed at understanding if the residual properties of carbon/epoxy specimens are affected by the infliction of electro-magneto-mechanical damage, and if there is a set of particular conditions such as loading case, strike intensity or presence of the fastener that are particularly critical for the material. The accuracy of the testing technique adopted as compared to real lightning strike events is fundamental question, and it has been discussed for decades. Previous work by NASA, FAA and Industry has led to the development of a recommended procedure, the SAE ARP 5412 [10] discussed above, which is accepted internationally as the sole test standard by which to

Table 1
Typical lightning strike levels and the airframe requirements.

Threat	Criteria	Requirement
High energy strike	Rare lightning strike 50–200 kA	Striking level in accordance to zoning diagram Continued safe flight (70% DLL) Ready detectable damage
Intermediate energy strike	Medium lightning strike 30–50 kA	Repair needed (100% DLL) Visible damage
Low energy strike	Nominal lightning strike 10–30 kA	No repair needed (150% DLL) Non or barely visible damage

simulate lightning strike in a laboratory environment. The research presented here follows accurately the recommendations contained in [10].

2. Experimental procedure

2.1. Description of the lightning strike generator and strike test setup

The lightning strike generator developed at the University of Washington is comprised of a high voltage capacitor, a high voltage resistor, an adjustable resistor stack, a spark gap switch, the test specimen and the current return network, as shown from the bottom up in Fig. 3. The capacitor is capable of supplying 44 kV and 52 μF, the adjustable resistor stack is used to vary the amperage of the strike and to modulate the waveforms, while the spark gap switch is used to trigger the strike. The area in proximity of the test specimen is reported in more detail in Fig. 4 and, from the bottom up, shows the dielectric support frame, current measuring device used to record the waveform, the conical copper striker, the CFRP coupon with the fastener, and the copper strips used to connect the specimen to the ground. The CFRP specimen is supported at the two short ends between two copper electrodes, whose position is adjusted to be in close contact with the specimen, and are encapsulated by non-conductive phenolic composites. The generator is contained in a chamber, which is electrically and physically separated from the surrounding environment in order to ensure safe operation.

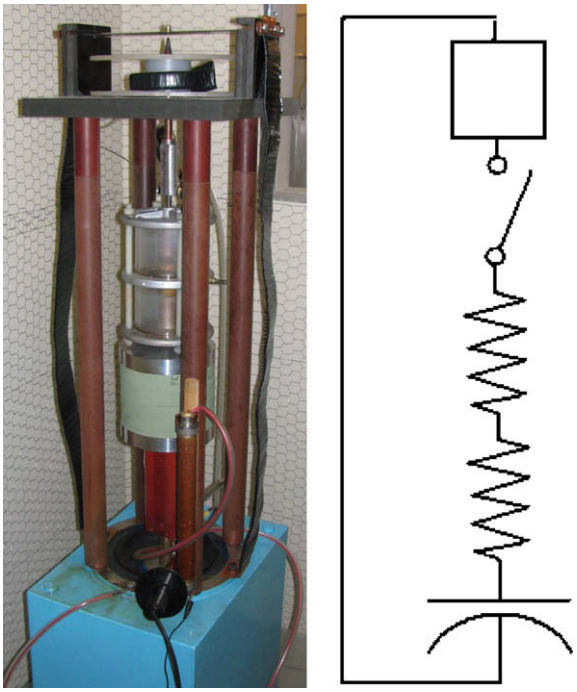

Fig. 3. Picture and schematics of the lightning strike generator.

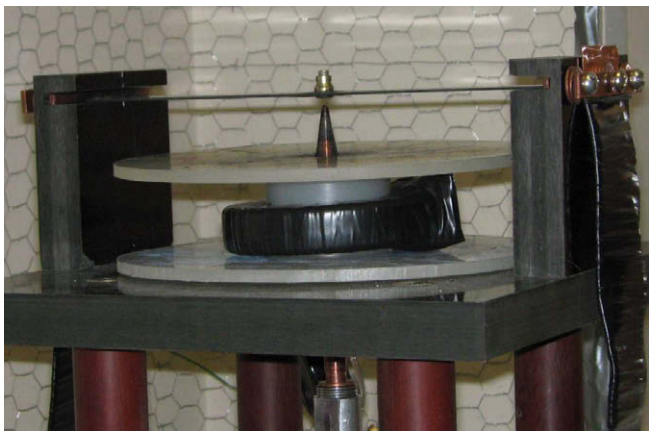

Fig. 4. Detail of the strike and test specimen area of the lightning strike generator.

The lightning strike generator is capable of generating waveform D as specified in SAE ARP 5412 [10]. Waveform D is designed to represent a typical restrike, after the primary strike to the airframe, and is also used to certify the vast majority of the airframe acreage. Waveform D calls for a maximum of 100 kA, released over less than 0.5 ms, and an action integral of 250×10^3 A^2 s, Fig. 2. However, strikes of 100 kA prescribed by waveforms D are typically used to strike full-scale test articles or subcomponents that are representative of actual hardware, but are far too high a current to be used to inflict damage in coupon-sized articles, such as the ones used in this study. For this study, strikes at 10, 30 and 50 kA are used to inflict different states of damage to the coupons, corresponding to 2.56, 23.80, and 49.86×10^3 A^2 s, respectively. The current intensity vs. time waveforms for all three strike levels are shown is Fig. 5, and show that all values are in line with the ones reported in [6,12].

Striker distance is kept constant for all tests at 0.125 in. (3.2 mm). Although at maximum voltage the generator is capable of striking targets as far as 1.5 in. (38.1 mm) away from the striker tip, this distance decreases rapidly for decreasing voltage. While it would be desirable to keep this distance as great as possible to allow for the formation of a longer arc, it is not possible to break down the air gap between striker and CFRP specimen at low voltages. Hence, for all three strike levels considered in this study, this gap is kept constant at the maximum value that the lowest current (10 kA) can break down. It is believed that the resulting damage state in the CFRP specimen will be affected if the striker distance were to be varied depending on the voltage, but further work will provide support to this idea.

The lightning strike generator is used to inflict damage in the CFRP specimens, in order to assess their damage resistance behavior, in a fashion very similar to that of low-velocity impact damage. The damaged specimens are then tested for residual strength and stiffness to assess their damage tolerance behavior, in a fashion also very similar to that of FOD damage or machined stress concentrations (notches).

2.2. Specimen fabrication and residual performance test set-up

Flat panels of CYCOM/FIBERITE G30-500 12K HTA/7714A carbon fiber/epoxy composites are fabricated by press molding for 60 min at 250 °F (121 °C). The lay-up is [+45/02/−45/03/90]s, for a total of 16 plies and a nominal ply thickness of 0.007 in. (0.18 mm). After molding, test coupons are machined with a diamond-coated water-cooled disk saw to the final dimensions of 12 in × 1.5 in (304.8 mm × 38.1 mm). These dimensions are chosen since they represent the bases for all unnotched tension (UNT) and compression (UNC), as well as filled-hole tension (FHT) and compression (FHC) test standards used by Boeing [11–13]. The specimens are tested as-molded, unpainted and unprotected. Although not representative of a flight-ready composite airframe structure, this configuration allows for focusing on the details of the CFRP material response to high electrical discharges alone. For the FHT and FHC specimens, 0.250 in. (6.35 mm) holes are drilled using a diamond-coated drill bit, and aircraft-grade stainless steel Hilok fasteners are subsequently installed. A total of 60 specimens are manufactured, of which 48 are tested

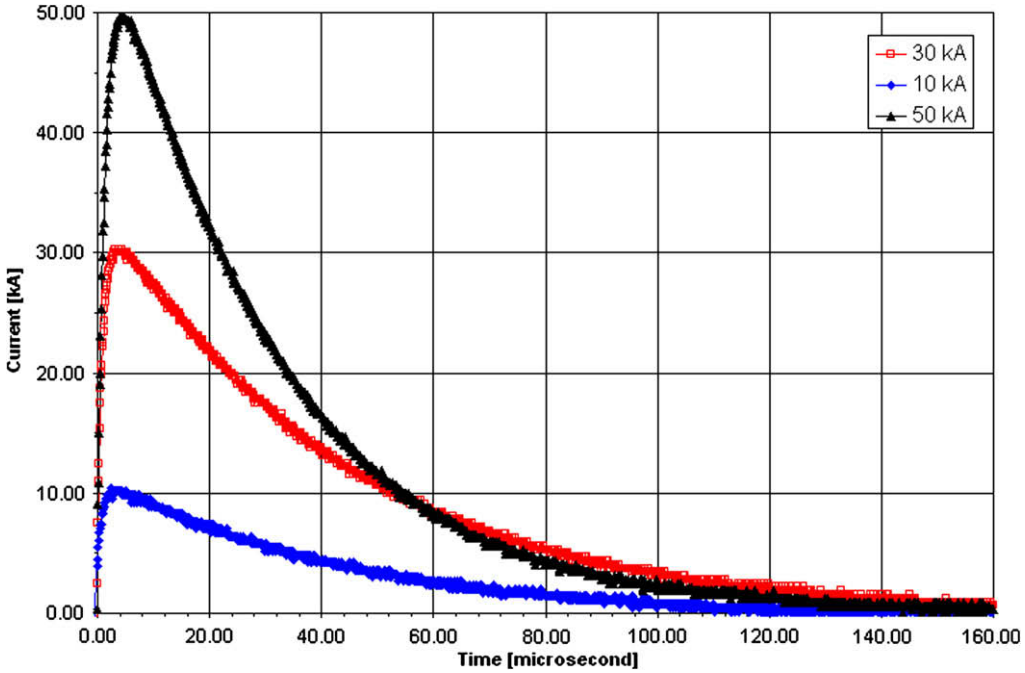

Fig. 5. Typical current waveforms generated in this study.

in a quasi-static test frame in tension and compression both in pristine and post-lightning strike condition, while the other 12 are used for destructive inspection. Pristine specimens are tested to obtain reference values for both strength and modulus. Table 2 summarizes the test matrix developed in this study.

Non-destructive inspection is performed on 100% of the pristine and damaged specimens via pulse-echo ultrasound using a C-scan system with a 5 MHz sensor. The projected damage area is then estimated using image analysis software. Destructive inspection is performed by cross-sectioning and optical microscopy of the lightning-damaged specimens. Two specimens for each current level, both unnotched and filled-hole, for a total of 12 specimens are inspected via microscopy. Multiple micrographic coupons are extracted from a single test specimen in order to reconstruct a full view of the damage through the thickness, both in proximity of the strike point and away from it. Advanced inspection methods, which employ special dyes and ultraviolet light to enhance the presence of damage [14,15], are described in subsequent sections.

Residual strength and stiffness are measured using 12 in. × 1.5 in. (304.8 mm × 38.1 mm) Boeing standard specimens [11–13]. Although it is recognized that the short dimension of this type of specimen is very small, and it may introduce complex finite-width effects both in the damage formation stage and residual strength stage, previous investigators in this area of research [6] have employed them as they represent the only possibility to test the effects of damage on coupon-sized specimens. Similar limitations are also known for the larger plate-like compression-after-impact specimen, which is used mostly to screen materials and derive qualitative trends rather than generating design values.

3. Results

3.1. Damage infliction

The strikes produce a loud sound, similar to that of a detonation, and generate a short, bright light, followed by a cloud of fire and sparks, likely due to the incandescent blast wave charged with carbon fiber and epoxy particles. Fig. 6 is extracted from a digital video recording at the time of peak current during the strike. However, if a digital camera with an exposure time longer than the

Table 2
Summary of details for all test configurations and results.

Family	Residual test	Width	Nominal thickness (in.)	Fastener diameter (in.)	Current (kA)	Repetitions
A	UNT	1.5	0.112	–	0	3
B	UNT	1.5	0.112	–	10	3
C	UNT	1.5	0.112	–	30	3
D	UNT	1.5	0.112	–	50	3
E	UNC	1.5	0.112	–	0	3
F	UNC	1.5	0.112	–	10	3
G	UNC	1.5	0.112	–	30	3
H	UNC	1.5	0.112	–	50	3
I	FHT	1.5	0.112	0.250	0	3
J	FHT	1.5	0.112	0.250	10	3
K	FHT	1.5	0.112	0.250	30	3
L	FHT	1.5	0.112	0.250	50	3
M	FHC	1.5	0.112	0.250	0	3
N	FHC	1.5	0.112	0.250	10	3
O	FHC	1.5	0.112	0.250	30	3
P	FHC	1.5	0.112	0.250	50	3

duration of the strike itself, and a series of polarized filters that reduce the intensity of the lighting are employed, it is possible to actually reduce the amount of "noise" in the image and focus on the central portion of the electrical channel, Figs. 6 and 7.

Both unnotched (or pristine) and filled-hole specimens are tested. Unnotched specimens exhibit increasing external damage for increasing current intensity, Fig. 8. Damage manifests as visible fiber fracture in the outer ply oriented at 45 °, as well as longitudinal splitting and bulging of the area around the strike, Fig. 9. In some cases the upper ply or plies even separate in small chips or fragments and leave an empty space on the surface. In general however, the damage appears to be confined to the surface of the specimen and in the region immediately surrounding the strike zone. For the given specimen, boundary conditions and loading configuration, damage does not reach the backface of the specimen. The visible damage area appears to be almost identical

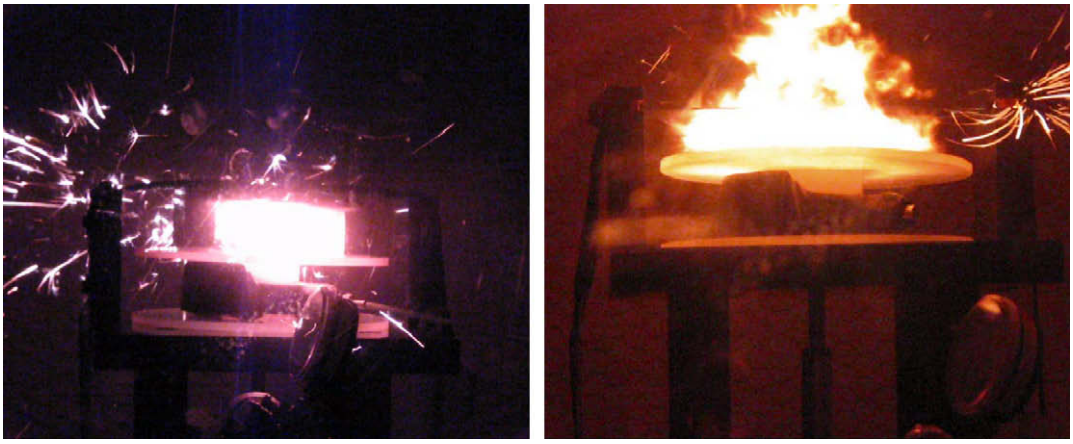

Fig. 6. Still image extracted at peak intensity from a video recording of a 50 kA strike.

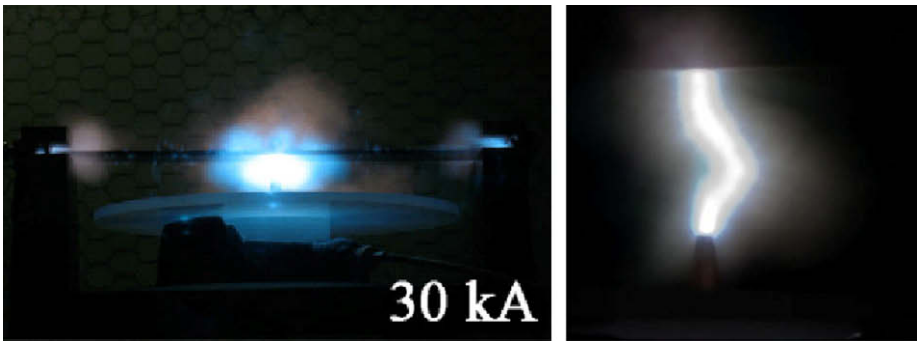

Fig. 7. Details of the strikes at 30 kA, obtained using a digital camera with a long exposure time and a system of polarized lenses to reduce the intensity of the light.

Fig. 8. Typical unnotched specimens, from pristine at the bottom to maximum current at the top.

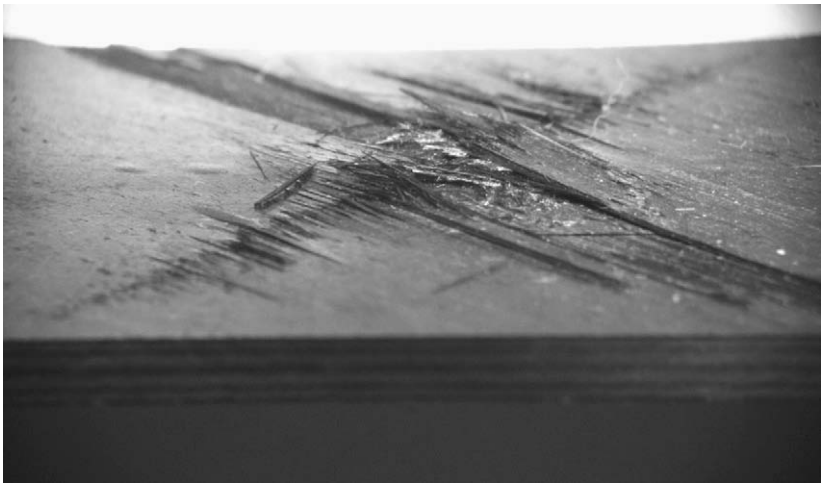

Fig. 9. Close-up of surface damage for unnotched specimens at 50 kA.

between the 30 and the 50 kA strikes, but caution should be exercised in interpreting these results. The finite width of the specimen imposes limitations on the propagation of damage, and hence these results cannot be extrapolated to larger panels, which will be the focus of future research.

Ultrasonic images for a representative unnotched specimen for each of the strike levels are reported in Fig. 10. The circular object appearing on the side of each specimen is a dime (USD 0.10) that is used for reference during the ultrasonic scan. Fig. 10 shows the shape of the damage area, which tends to be elongated in the direction of the fibers in the outer ply, and reports a calculated damage area. Although there appear to be a clear trend of increasing projected damage area for increasing current intensity, the size of the damage areas for the 30 and 50 kA strikes are relatively similar. Beyond 10 kA, the damage area reaches the boundaries of the specimen and is then forced to grow longitudinally. However, with these finite-width limitations in mind, it is possible to perform quantitative comparisons between specimens, and obtain the plot in Fig. 11. For the unnotched specimen it appears that the projected damage area increases linearly up to 30 kA, and then levels off, for the reasons mentioned before. From the plot it can be seen

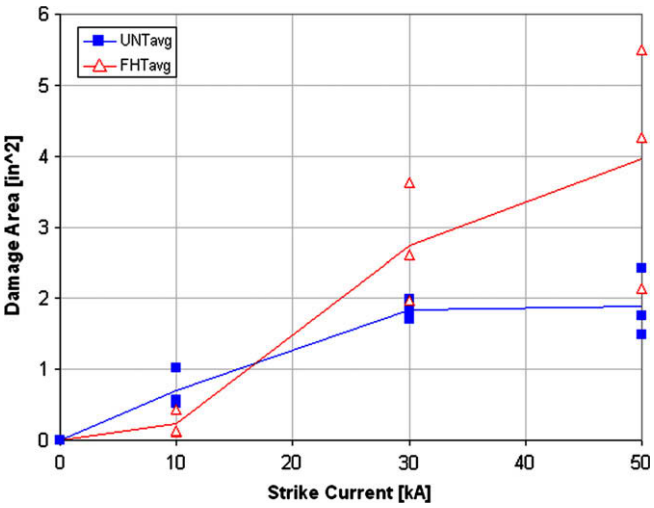

Fig. 11. Projected damage area for unnotched and filled-hole specimens.

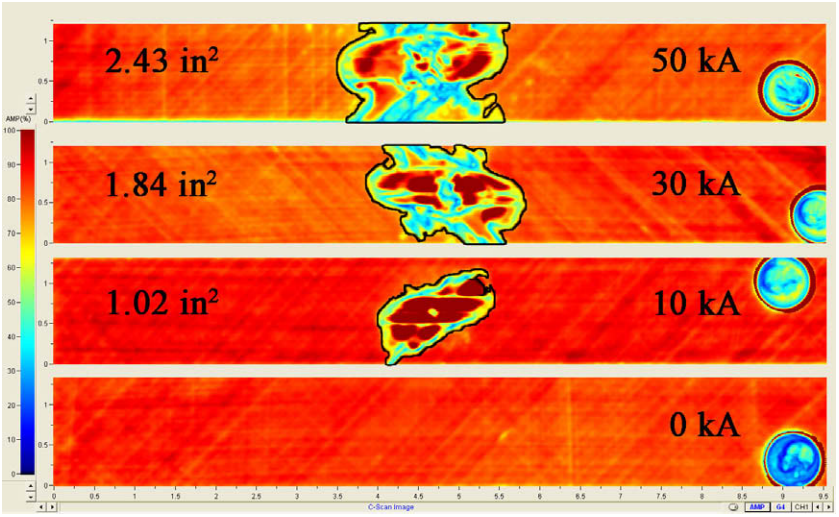

Fig. 10. Projected damage area obtained via C-scan for unnotched specimens.

that for each test repetition, three specimens per current level, there is noticeable variation in the measured area, but it appears to be within acceptable values.

For filled-hole specimens the results are dramatically different. For 10 kA strikes, the only damage visible is surface pitting of the fasteners on the head side, where the strike takes place, Fig. 12. However, for the 30 and 50 kA strike the surface damage is much more extensive than in the unnotched specimens, Figs. 12–14. Besides pitting of the fastener, severe bulging of the plies toward the surface is visible in the proximity of the fastener, and extensive fiber breakage observable on both top and back faces. Entire laminate segments delaminate throughout the thickness of the specimen, and in some cases even split and detach from the bulk of the specimen itself. At 50 kA, the fastener appears to sink inside

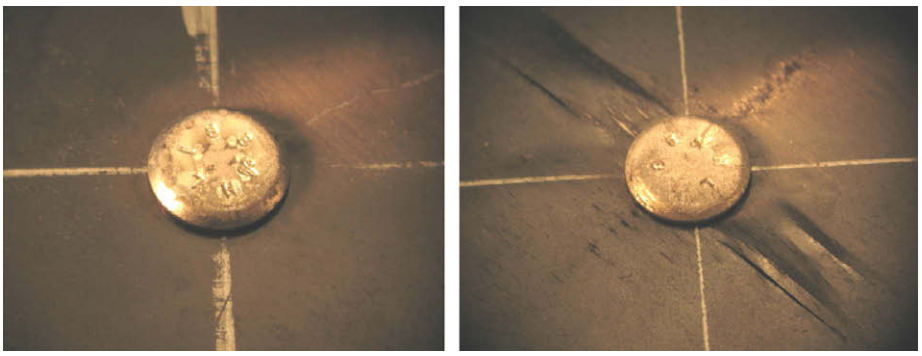

Fig. 12. Close-up of top surface fastener and laminate damage for filled-hole specimen at 10 and 30 kA.

Fig. 13. Typical filled-hole specimens, from pristine at the bottom to maximum current at the top.

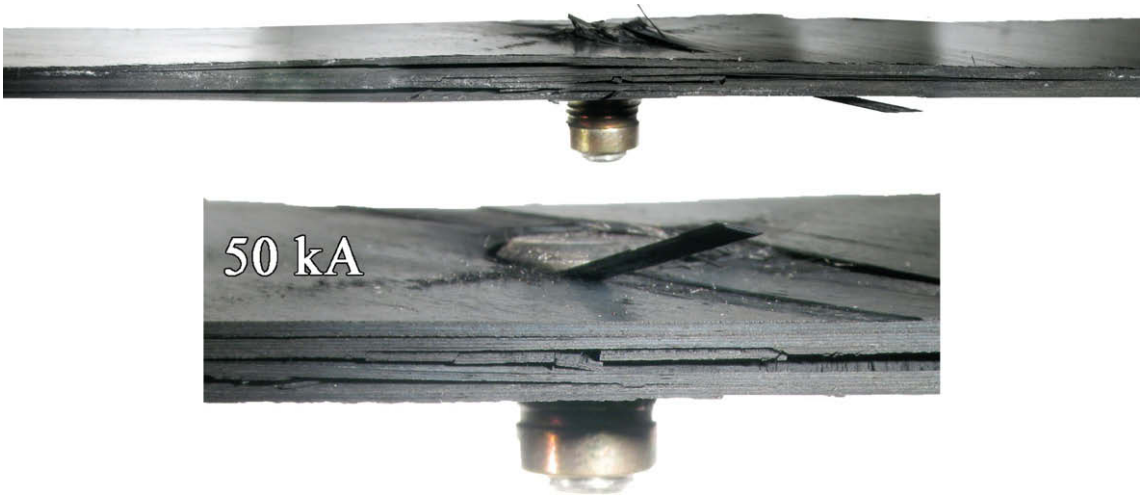

Fig. 14. Close-up of edge/top surface damage for filled-hole specimen at 50 kA (different sides shown).

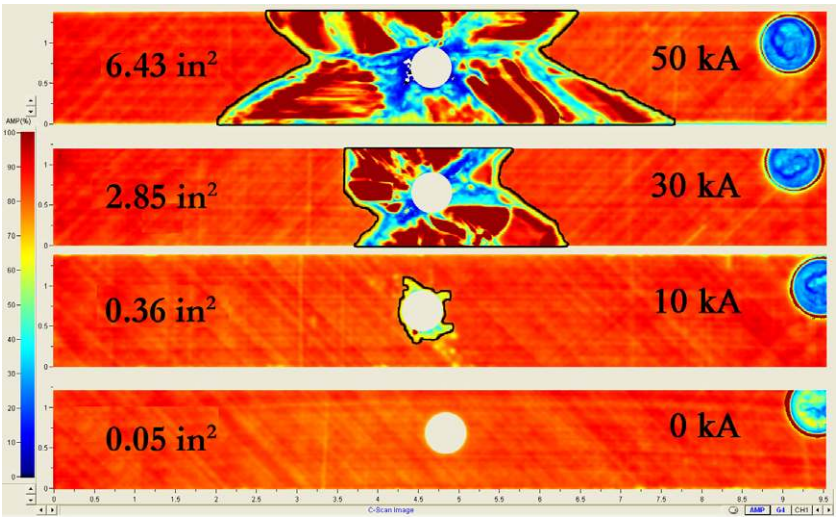

Fig. 15. Projected damage area obtained via C-scan for filled-hole specimens.

the top plies of the laminate. In general, the damage on the surface of the filled-hole specimens appears to be due mostly due to acoustic shock, hence the large bulging of the upper plies, rather than burning of the matrix on the surface, as for the unnotched specimens.

Ultrasonic images for a representative filled-hole specimen for each of the strike levels are reported in Fig. 15. In the pristine specimen the fastener appears as a white round, with an area of 0.05 in^2 (32.2 mm^2) approximately. Fig. 15 confirms that for the 10 kA strike the damage area is contained in the fastener itself, or in the immediate proximity of the fastener hole. For 30 and 50 kA strikes, however, there appears to be a radical increase in damage area, and at 50 kA the vast majority of specimen appears to be damaged. From the ultrasonic image it is only possible to obtain information about a projected damage area; hence, to further identify the location and nature of the damage it is necessary to inspect the cross-section via micrography, as discussed later in the paper. Once again it is important to remember that the energy used to inflict damage exceeds the amount that the specimen can contain within its short width, and hence the damage is forced to grow longitudinally.

Trends observed in projected damage area for filled-hole specimens are reported in Fig. 11, together with the unnotched ones. For filled-hole specimens, the damage area is very small for the 10 kA strikes, but there is a clear inversion in the trends observed for the 30 and 50 kA strikes, where it rapidly grows to larger values than the unnotched specimens. While initially the damage area appears to grow at a slow rate, between 10 and 30 kA there is a sharp increase, and even between 30 and 50 kA strikes the area appears to grow substantially, albeit at a lower rate. The steel fastener appears to act as an electrical damage sink for the low current levels, whereby it absorbs the majority of the damage, but at the higher current levels it appears to become an amplifier, thus distributing the load throughout the entire laminate rather than containing it on the outer plies.

It should be noted that the variation in damage area measurements for the filled-hole specimens is much greater than for the unnotched ones, and in particular it becomes nearly unacceptable at 50 kA. It is suggested that fastener fit may have a fundamental role in introducing the electrical load in the surrounding laminate, and hence the quality of the fit may be responsible for the great variation observed. Future work will have to focus on the fundamental role of the metallic fastener in the formation of damage.

3.2. Residual strength

After inflicting damage onto the specimens, these are tested to failure in tension or compression to quantify the loss in mechanical performance due to the presence of damage. For both pristine and filled-hole specimens, strength is calculated as the ratio of the maximum load divided by the gross section, consistently with aerospace practice [6,12,13,16].

Residual strengths for UNT and UNC specimens, families A–D and E–H, respectively, are shown in Fig. 16. It is interesting to observe that at the maximum energy level, 50 kA, the reduction in tensile strength is approximately 20%, while in compression it is slightly over 30%. Unnotched residual strength for both tension and compression decreases in a relatively linear fashion with current intensity. These values are the averages of three test specimens per family. Residual modulus measurements are plotted in Fig. 17, and shows that, both for UNT and UNC, modulus appears to remain nearly constant in the entire range of currents. Even at 50 kA the decrease is minimal, but large variation in the data is visible. It is counterintuitive that the elastic response of the damaged specimens is not affected to a greater extent by the presence of damage, particularly in compression.

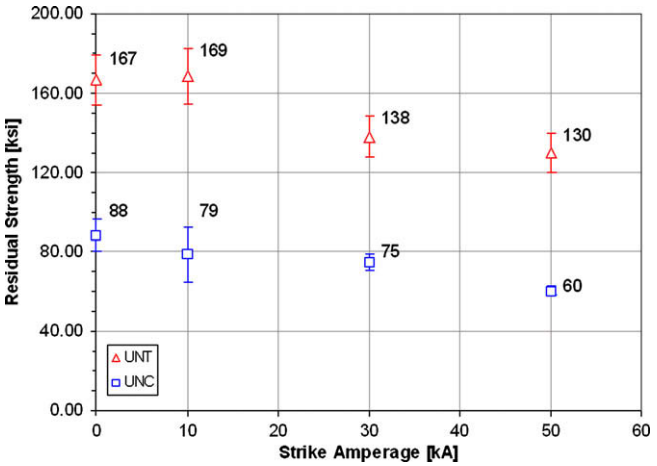

Fig. 16. Residual tension and compression strength plot as a function of current intensity for unnotched specimens.

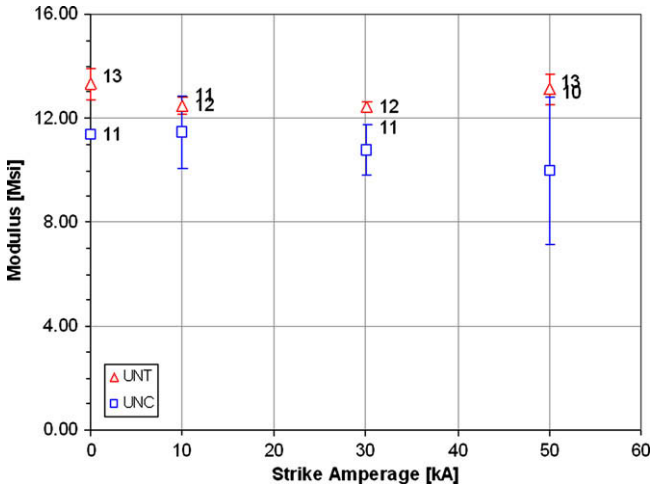

Fig. 17. Residual tension and compression modulus plot as a function of current intensity for unnotched specimens.

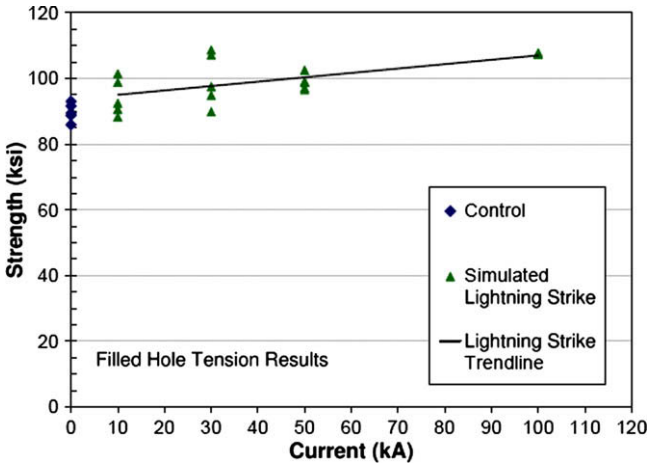

Fig. 19. Increase in residual strength with increasing current for filled-hole tension specimens reported in [6].

FHT and FHC results are reported in Fig. 18. Average strength values for FHT appear to increase with increasing damage state, up to 13% for 30 kA, then decrease back to the pristine value for the 50 kA specimens. Initially these results may seem surprising, but previous results published by Boeing [6] appear to confirm the observation of increasing FHT strength with lightning strike damage. In [6], FHT specimens having the same geometry as those of this study are show a clear trend of increasing apparent strength after strike, Fig. 19. Noticeable scatter is present in their data, as well as in the current investigation. It should be noted that the specimens used in [6] are stitched AS4/3501-6 resin film infused deriving from the NASA advanced composites technology (ACT) program, and are substantially thicker than the ones used in this investigation. Nonetheless, for both specimen types it is thought that the lightning strike damage surrounding the fastener acts as to relieve the stress concentration around the hole in a fashion not too different from that of the damage zone evolution reported by several authors during testing of open- or filled-hole specimens [16,17].

For the FHC specimens, also reported in Fig. 18, the results also appear to slightly increase for the 10 kA strike, then rapidly drop by as much as 65% for 50 kA. It appears therefore to be confirmed that the fastener has an extremely significant role in both the damage resistance and damage tolerance response of the CFRP specimens.

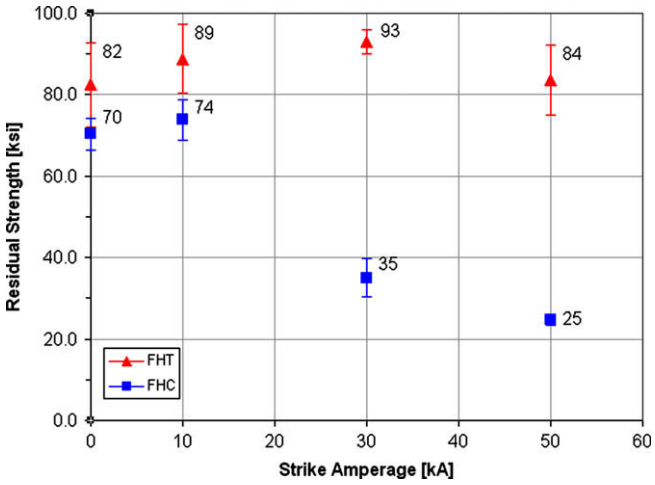

Fig. 18. Residual tension and compression strength plot as a function of current intensity for filled-hole specimens.

4. Microscopy

The zone in and around the strike is very fragile due to the broken fibers and vaporized matrix, as shown in Figs. 9, 12 and 14. Care must be taken in cross-sectioning and mounting in order to preserve much of the critical information [14,15]. Mounting and sectioning lightning strike composite specimens are best accomplished with a two-stage mount, Fig. 20. It is advisable to add a

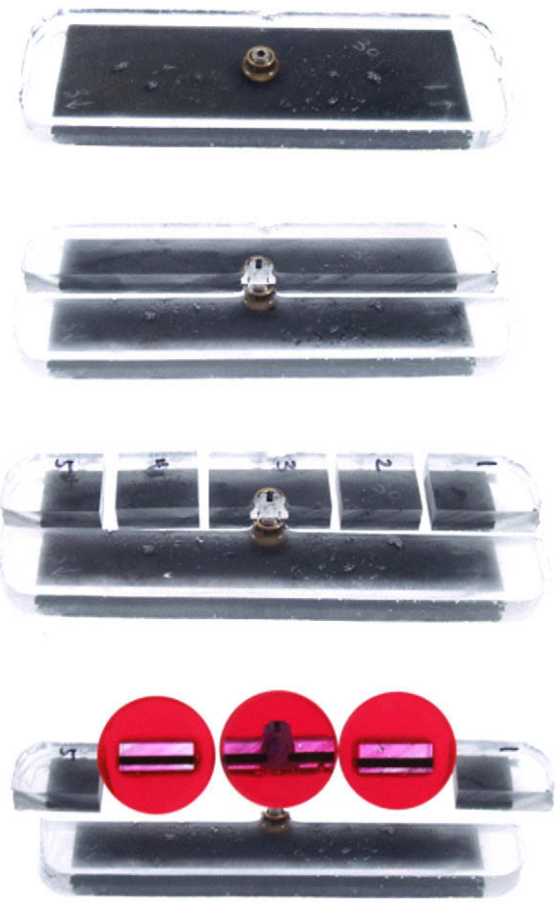

Fig. 20. Mounting and polishing procedure employed for microscopy of specimens subjected to lightning strike.

dye to the mounting epoxy, such as rhodamine-B laser dye, which gives a red-orange tint to the mounting resin. The use of a laser dyed back filled epoxy is very important so that the vaporized zone is preserved and apparent with the fluorescence, leaving no doubt which are the composite polymer and the mounting polymer. Without the dye, the features can be so subtle and contrast very low such that features can go undetected. The strike area of the specimen is first vacuum-impregnated with the epoxy, then pressure-cured to minimize formation of air bubbles. The encapsulated area preserves the fragile material in place. The specimen is prepared with a 6-step process: 180 grit, 600 grit, 1200 grit, 9 μm, 3 μm silk, 3 μm non-nap polyester and ending up with 1 h polishing with a non-nap polyester cloth and 10% alumina solution [14,15]. After final mounting, the specimen is coated with a dye, which is absorbed by capillary action into features such as microcracks. Microstructural analysis can be performed with bright field, polarized light, dark field, and epi-fluorescence, Fig. 21. When viewed with polarized light or epi-fluorescence, the dyed features will be easily observed.

The microstructure of polymer composites that have been exposed to high energy strike is quite different and can vary widely depending on the polymer. The strike affects in thermoset polymers usually have a central hot spot zone where the fibers are degraded and a surrounding zone where the polymer is vaporized or degraded. A transverse microcrack, hot spots and burn mark in a cross-section of a specimen are shown in Fig. 22, in relative proximity of the strike area but toward the center of the laminate (9th ply). Although the damage is visible in brightfield (left), it becomes apparent after exposure to UV light and with the aid of the exitation filter and dye penetrant (right).

Detailed analysis of the microscopic damage is beyond the scope of this study and will be the subject of a separate publication. However, low magnification stereomicroscopy is used here to further assess the extent and location of the damage at the mesoscopic level, to complement the observations performed at the macroscopic level via visual and ultrasonic inspections. Figs. 23–28 report the cross-sectional view of the damage at the central point of the strike for each representative family of unnotched and filled-hole specimens, at 10, 30 and 50 kA strikes.

For 10 kA unnotched specimens, Fig. 23, the section shows partial obliteration of the +45° surface ply, and a major delamination running at the interface between 3rd and 4th ply. The two 0° plies appear to remain intact and separate from the adjacent −45° ply, suggesting that the mismatch in electrical resistance between the different orientation plies has a significant role in the distribution of the current, and hence damage, in the laminate.

For 30 kA unnotched specimens, Fig. 24, the top +45° surface ply is completely obliterated and separated from the laminate, the adjacent 2nd and 3rd 0° plies remain intact but burst open toward the outside, and the 4th −45° ply appears to be also completely obliterated. A major delamination appears to run along the interface between the 4th and the 5th ply, which is the first of a three 0° stack. The remaining part of the specimen appears intact.

The situation for the 50 kA unnotched specimens, Fig. 25, is very similar and again shows that the interface between plies with low electrical resistance in the direction of the current flow (such as the 0° stacks) and higher resistance plies (±45°) constitutes the preferred path for the formation of the large delaminations visible in the ultrasonic images.

Ten kiloamperes filled-hole specimens, Fig. 26, appear to show no damage through the thickness, and the minimal damage area observed in the ultrasonic scan in some of the specimens is confined to a partial resin burn-off on the top ply around the fastener.

Thirty kiloamperes filled-hole specimens, Fig. 27, exhibit quite a different behavior than any previous ones, and show different

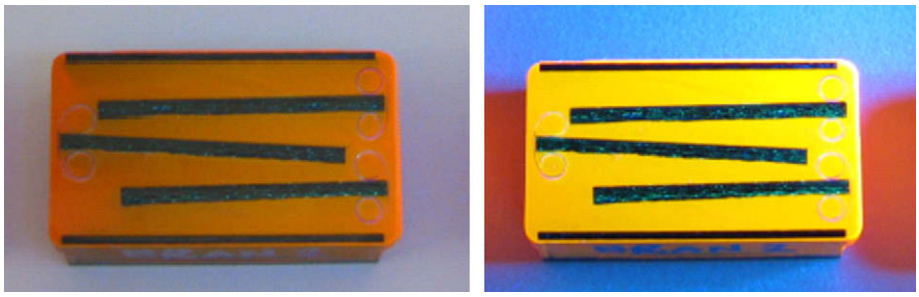

Fig. 21. Specimen mounted in epoxy resin with laser dye under regular light (left) and under UV light after application of dye penetrant (right).

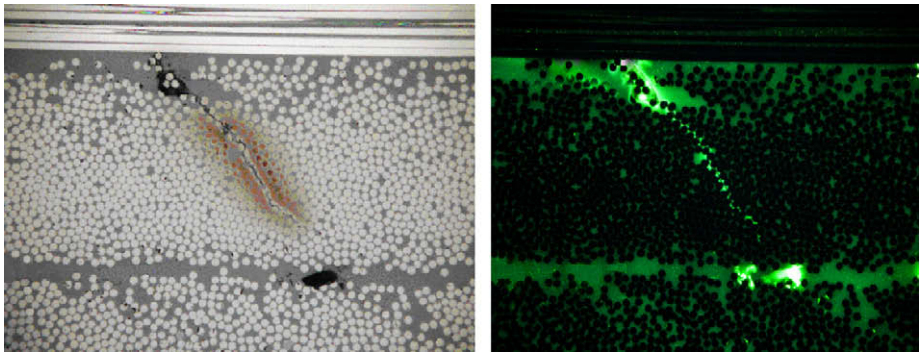

Fig. 22. High magnification micrograph of localized area of pyrolized fibers and vaporized matrix in specimen after 50 kA strike under brightfield (left) and UV light with dye penetrant (right).

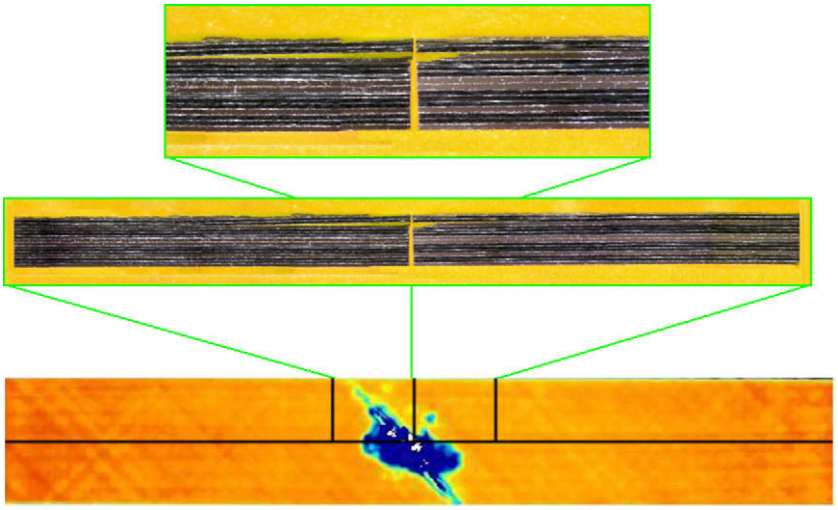

Fig. 23. C-scan and relative micrograph of 10 kA strike unnotched specimen.

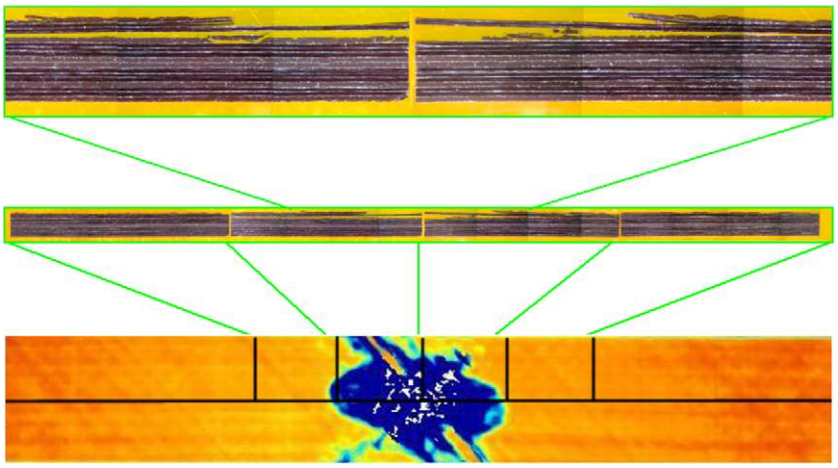

Fig. 24. C-scan and relative micrograph of 30 kA strike unnotched specimen.

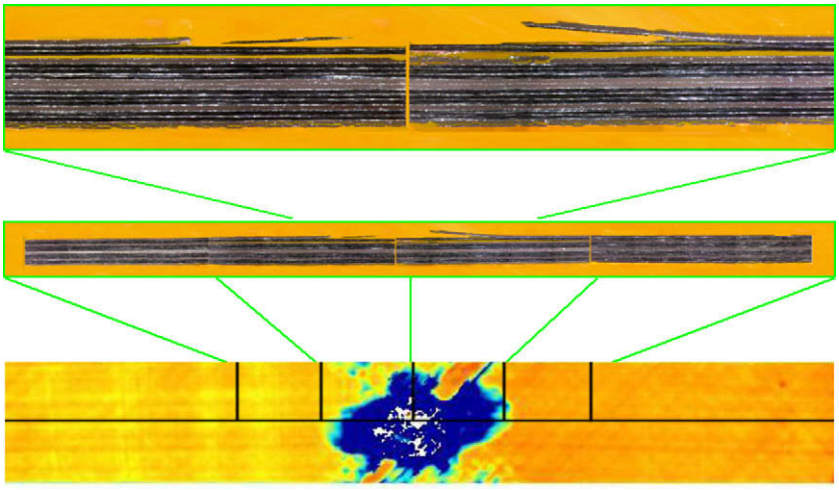

Fig. 25. C-scan and relative micrograph of 50 kA strike unnotched specimen.

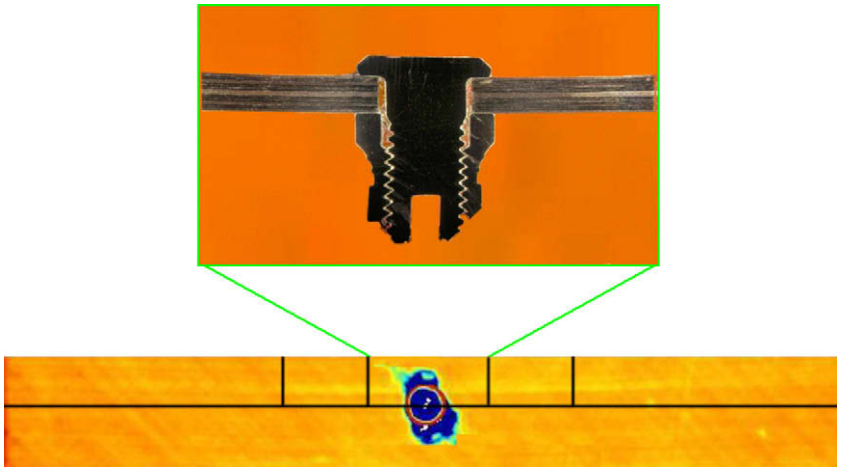

Fig. 26. C-scan and relative micrograph of 10 kA strike filled-hole specimen.

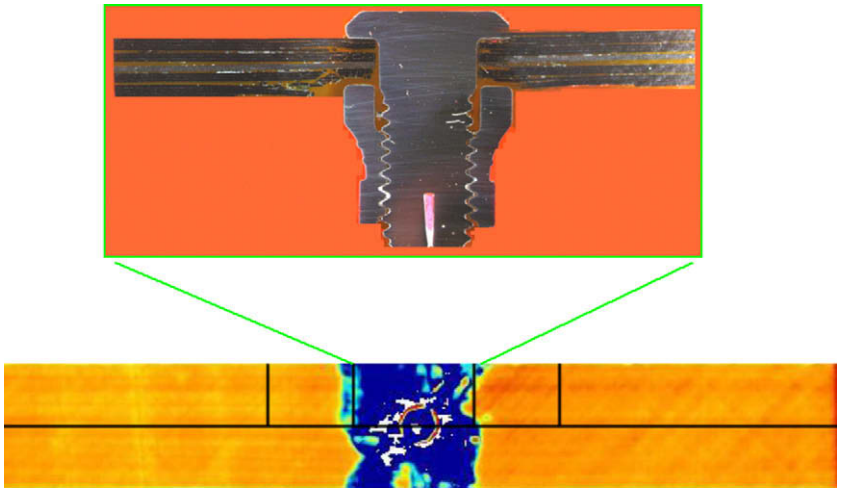

Fig. 27. C-scan and relative micrograph of 30 kA strike filled-hole specimen.

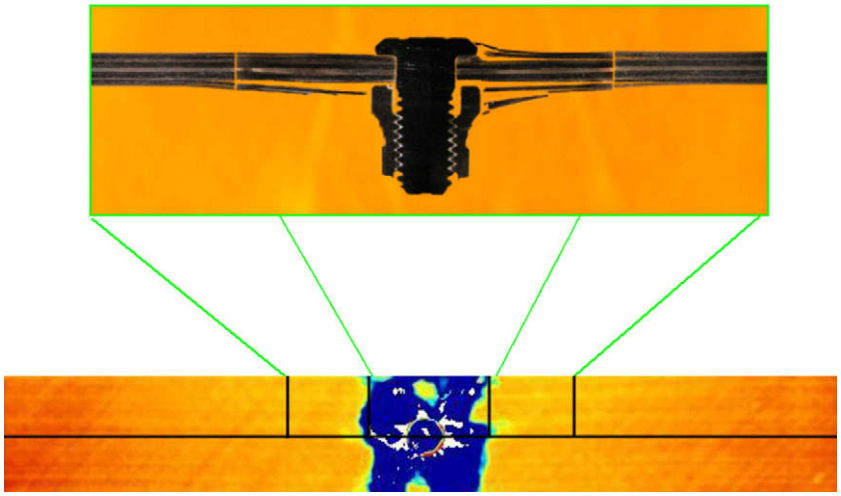

Fig. 28. C-scan and relative micrograph of 50 kA strike filled-hole specimen.

delamination paths through the thickness of the laminate. These are visible mostly at the interface between 0-ply stacks and either ±45° or 90° plies. Complete obliteration of the resin and fibers is observable on the backface of the laminate, in proximity of the fastener collar. Partial fragmentation of 0° ply stacks is also observable, and suggests that the fastener has the effect of distributing the electrical load to all the plies in its contact or proximity.

Fifty kiloamperes filled-hole specimens, Fig. 28, show even more extensive damage, with both top and bottom plies splaying outward, and extensive delamination fronts at all interfaces between high and low conductivity plies. Integrity of the specimen is completely compromised.

5. Conclusions

Unnotched and filled-hole CFRP specimens were subjected to simulated lightning strike damage at different current levels. The strikes were performed using a lightning strike generator purposely developed following current aerospace industry practice. After damage was inflicted, the CFRP specimens were tested for residual strength and modulus in tension and compression. In general, filled-hole compression strength appears to be the most affected property, with dramatic decreases for the 30 and 50 kA strikes. Visual inspection and ultrasonic scans show that the damage inflicted on the filled-hole specimens is much greater than for the unnotched ones above the 10 kA level, where instead the damage remains confined to the fastener. Optical microscopy confirms that for unnotched specimens the damage is confined to the upper two–four plies, while for filled-hole specimens it is either confined to the fastener alone at the lowest applied current, or it affects the entire thickness of the laminate up to the backface at the higher applied currents. The complex damage state inside the laminate comprises pyrolized fibers, vaporized resin, and traces of inter- as well as intra-ply arcing. These damage mechanisms will require further investigation. The different behavior of the specimen in presence of the fastener suggests that particular care needs to be ensured for fastened joints with regards to lightning strike. While damage to unnotched airframe skins will lead to moisture ingression an ultraviolet light exposure of the fibers but remains contained to the outer plies, damage to skins containing a fastener will lead to through-thickness perforation and subsequent loss of pressurization, as well much lower residual strength.

Acknowledgments

The authors would like to acknowledge engineers Art Blair and Robert Gordon, Prof. Tom Mattick, and undergraduate research assistants Andy Le, Parker Davis, Dave Medendorp, and Andrew Southworth for their help in building the generator and conducting the experiments. They would also like to thank Diane Heidlebaugh and Art Day (Boeing Phantom Works), and Rob Steinle (Boeing Commercial Airplanes) for their technical support and experienced advice. Dr. Al Miller and Dr. Patrick Stickler (Boeing 787 Technology Integration) are also gratefully acknowledged. The material for this study was supplied by Shreeram Raj of Cytec Engineered Materials.

References

[1] Miller A. The Boeing 787 dreamliner. Keynote address. In: 22nd American society for composites technical conference, Seattle, WA; September 2007.
[2] Rupke E. Lightning direct effects handbook. Report no. AGATE-WP3.1-031027-043-Design guideline, March 1; 2002. Lightning Technologies Inc.
[3] Fisher FA, Plumer JA. Aircraft lightning protection handbook. DOT/FAA/CT-89/22; September 1989.
[4] Welch J. Repair design, test and process considerations for lightning strike. In: Joint FAA-Boeing-Airbus damage tolerance workshop, Amsterdam, The Netherlands; May 2007.
[5] Welch JM, Kitt BR, Meusborn RJ. Honeycomb panel lightning strike testing: metal mesh product protection assessment. SAMPE J 2008(7/8).
[6] Heidlebaugh D, Avery W, Uhrich S. Effect of lightning currents on structural performance of composite materials. In: International conference on lightning and static electricity. SAE paper no. 2001-01-2885, Seattle, WA; September 2001.
[7] Fielding J. Incorporation of nanomaterials into polymer matrix composites for multifunctionality. In: AFOSR workshop on manufacturing/processing of multifunctional composite structures, Seattle, WA; September 2007.
[8] US DOT/FAA Advisory Circular AC 25-21. Certification of transport aircraft structures. Section 25.581 lightning protection; September 1999. p. 657.
[9] Aerospace Recommended Practice ARP 5414. Aircraft lightning zoning. SAE; 1999.
[10] Aerospace Recommended Practice ARP 5412. Aircraft lightning environment and related test waveforms. SAE; 1999.
[11] Boeing standard test method for unnotched tension. D6-83079-61, The Boeing Co.
[12] Boeing standard test method for open-hole tension. D6-83079-62, The Boeing Co.
[13] Boeing standard test method for unnotched and open-hole compression. D6-83079-71, The Boeing Co.
[14] Gammon LM, Hayes BS. The affects of lightning strikes and high current on polymer composites. Microsc Microanal 2002;8(Suppl. 2):1236–7.
[15] Gammon LM. Polymeric composites morphological characterization and fracture analysis: fluorescent, dark field, bright field, and polarized light optical microscopy. Microsc Microanal 2004;10(Suppl. 2):740–1.
[16] Laminate strength and failure – stress concentrations. Composite materials handbook. MIL-HDBK-17, Section 5.4.4, Rev. F, vol. 3; 2002 [chapter 5].
[17] Whitney J. Fracture analysis of laminates. Engineered materials handbook, vol. 1. Composites – ASM International; 1987. p. 252–7.